Available online at www.sciencedirect.com
ScienceDirect
Trans. Nonferrous Met. Soc. China 30(2020) 147−159
Transactions of Nonferrous Metals Society of China
www.tnmsc.cn

High pressure EIGA preparation and 3D printing capability of Ti−6Al−4V powder

Kuai-kuai GUO[1,2], Chang-sheng LIU[1,2], Sui-yuan CHEN[1,2], Huan-huan DONG[1,2], Si-yu WANG[1,2]

1. School of Material Science and Engineering, Northeastern University, Shenyang 110819, China;
2. Key Laboratory for Laser Application Technology and Equipment of Liaoning Province, Northeastern University, Shenyang 110819, China

Received 19 February 2019; accepted 15 November 2019

Abstract: Ti−6Al−4V alloy powder was processed by electrode induction melting gas atomization (EIGA) at high gas pressure (5.5−7.0 MPa). The effects of atomizing gas pressure on the powder characteristics and the microstructure, along with the mechanical properties of the as-fabricated block by laser melting deposition (LMD), were investigated. The results indicate that the diameters of powders are distributed in a wide range of sizes from 1 to 400 μm, and the median powder size (d_{50}) decreases with increasing gas pressure. The powders with a size fraction of 100−150 μm obtained at gas pressures of 6.0 and 6.5 MPa have better flowability. The oxygen content is consistent with the change trend of gas pressure within a low range of 0.06%−0.20%. Specimens fabricated by LMD are mainly composed of α+β grains with a fine lamellar Widmanstatten structures and have the ultimate tensile strength (UTS) and yield strength of approximately 1100 and 1000 MPa, respectively. Furthermore, the atomized powders have a favorable 3D printing capability, and the mechanical properties of Ti−6Al−4V alloys manufactured by LMD typically exceed those of their cast or wrought counterparts.

Key words: Ti−6Al−4V powder; high pressure gas atomization; particle size; flowability; 3D printing capability

1 Introduction

Ti−6Al−4V (TC4) has received increasing attention for additive manufacturing (AM) applications in aerospace and automotive fields because of its low density, superior corrosion resistance, ductility and high temperature deformation properties [1,2]. Production of spherical Ti-alloy powder can be accomplished by gas atomization (GA) [3,4]. The melting process for gas atomization can involve either vacuum induction melting or a rod that is liquefied by electrode induction melting (electrode induction melting gas atomization, EIGA) [5,6]. In the GA process, process parameters have an important influence on powder properties. Gas pressure is especially important in determining the particle size and physical properties. Studies involving the effects of gas pressure on powder properties have been carried out by many researchers. CHEN and WAN [7] and AKSOY and UNAL [8] found that the particle size decreased with increasing atomization pressure. ZHAO et al [9] studied the influence of low pressure on fine powders and cooling mechanisms. A high gas pressure was shown to result in a broader size distribution and the particles at a high gas atomization pressure exhibited a high cooling rate. However, few studies have focused on the effect of high pressure gas atomization.

Foundation item: Project (2017YFB0305801) supported by the National Key R&D Program of China; Project (U1508213) supported by the Joint-Fund of NSFC−Liaoning, China; Project (51771051) supported by the National Natural Science Foundation of China

Corresponding author: Chang-sheng LIU; Tel: +86-24-83687575; E-mail: csliu@mail.neu.edu.cn

DOI: 10.1016/S1003-6326(19)65187-3

Laser melting deposition (3D printing) capabilities are used to evaluate whether a material can be used for printing, which is similar to the workability of metals such as castability, forgeability and weldability. Unlike these traditional "material reduction" processing methods, the preparation and formation of metals can proceed from the three-dimensional data of CAD design and rapidly form complex solid materials or parts based on layer-by-layer addition. AM is an advanced processing technology with high processing speed, high integration and no limitation on the complexity of components. Laser melting deposition technology is an ideal preparation method for complex TC4 components applied in the aerospace industry due to the use of less material and energy, along with a low cost and short production cycle [10,11]. The metal powders used in AM have stricter requirements for the particle size distribution, sphericity, fluidity and oxygen content [12]. However, traditional preparation methods of titanium alloys, such as the reduction of metals and hydride−dehydride (HDH) processes, are used to prepare powders with irregular shapes and a high oxygen content [13]. Compared with the properties of the powders prepared by rotating electrode powder (REP)/plasma rotating electrode powder (PREP), the powders fabricated by EIGA are extensively distributed in different powder size fractions, and the particle size is finer, which is desired for laser melting deposition (LMD) applications [14,15]. Therefore, the preparation of Ti−6Al−4V powders with appropriate properties for LMD is necessary and promising.

High-pressure gas atomization is an efficient method of producing fine alloy powders [16]. This work aims at preparing Ti−6Al−4V alloy powder with high performance by EIGA at high-atomizing pressure, and the microstructures and defects of the powder were studied. These results are significant for understanding the relationship between powder properties and high pressure. Finally, the tensile properties of Ti−6Al−4V alloys manufactured by LMD were investigated to evaluate the 3D printing capabilities of self-prepared titanium alloy powders.

2 Exprimental

2.1 Preparation of TC4 alloy powder

TC4 alloy powder was produced using an EIGA powder manufacturing apparatus independently developed by Anshan Northeastern University Laser Technology Co., Ltd. (China). The equipment combines the advantages of gas atomization and electromagnetic induction melting to achieve continuous production of titanium alloy powder. For the EIGA experiment, Ti−6Al−4V bars (50 mm in diameter and 1000 mm in length) were used as the base metal. The induction melting power is 50−70 kW, and the electrode rotation speed is 15−40 (°)/s. The atomization pressure is 5−8 MPa. The atomizing chamber of the EIGA equipment was pumped to a high vacuum state until the vacuum degree reached 3×10^{-3} Pa. High purity argon gas with 99.999% purity was used as the atomizing gas. In experiment, different atomization pressures of 5.5, 6.0, 6.5 and 7.0 MPa were adopted. After the preparation process, the Ti−6Al−4V powders were extracted from the collection chamber.

2.2 Laser melting deposition additive-manufacturing of metal

The sample was fabricated by LMD in a system (IPG, SL−1GY−700D) consisting of a maximum output power of 800 W and a beam diameter of 3 mm with a ytterbium-doped fiber laser under argon atmosphere to minimize the oxygen contamination of the layer-by-layer Ti−6Al−4V substrate. The travel speed was 8 mm/s.

2.3 Characterization of TC4 alloy powder and mechanical tests

Powder particle size distribution was measured by a laser particle size analyzer (LA−920). The microstructure for EIGA powders was observed using a Shimadzu−SSX−550 scanning electron microscope (SEM). The surface roughness of the powder was measured using laser scanning confocal microscopy (OLYMPUS LEXT 3100). The phase of Ti−6Al−4V titanium alloy powder was analyzed by SmartLab−9000 type X-ray diffraction (XRD) with a scanning speed of 2 (°)/min. The oxygen content of the powders was measured by a nitrogen−hydrogen−oxygen analyzer (TCH−600). A HYL−102 Holzer flow meter was used to measure the apparent density and flowability of the powder. The as-fabricated LMD block is shown in Fig. 1(a). The geometry of the tensile plate specimen is shown in Fig. 1(b). Three

tensile plate specimens were cut perpendicular to the fabricating direction, as shown in Fig. 2. Tensile testing was performed on an electronic universal testing machine (AG-Xplus) with a 100 kN capacity.

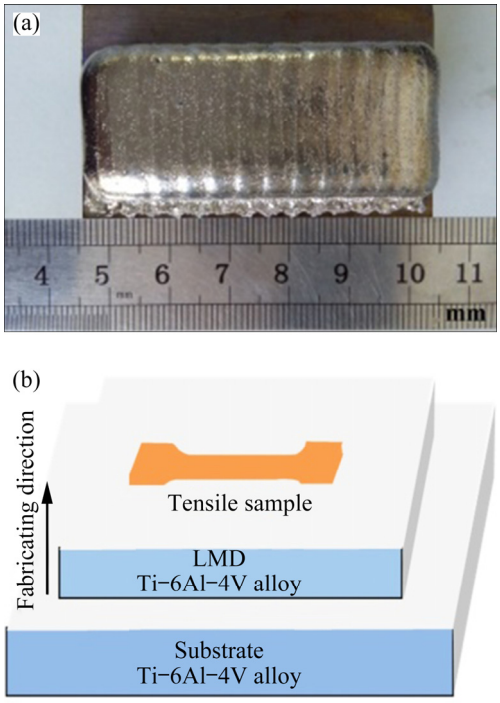

Fig. 1 As-fabricated LMD block (a) and schematic diagram of tensile specimens extracted from component (b)

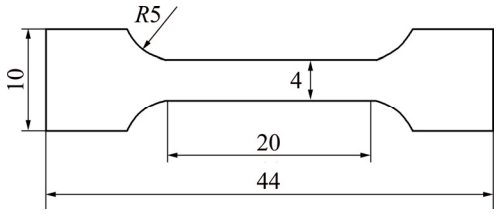

Fig. 2 Dimensions (in mm) of tensile plate specimen

3 Results and discussion

3.1 Particle size distribution (PSD) and microscopic morphology

The effect of gas pressure on the size of the produced TC4 powder is presented in Fig. 3(a). The data show that as expected, the size distribution curves move to the left with increasing gas pressure, which means a decrease of powder size. This is due to the influence of the secondary breakup [17]. The atomization process is mainly divided into three stages [18]: in the first stage, the impacted metal droplets are torn and pulled into a wavy metal film away from the center by a high-speed gas; in the

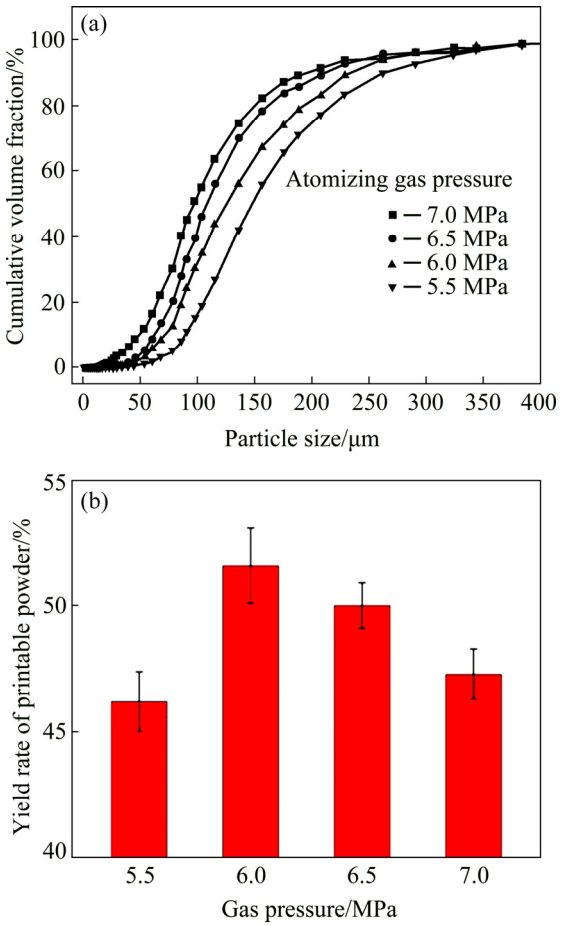

Fig. 3 Particle size distribution of TC4 powder prepared at different gas pressures: (a) Cumulative volume fraction; (b) Yield rate of printable powder

second stage, due to the movement of the gas flow, the wavy metal film is not stable under the reaction of the liquid surface tension, the thin film that is held in place contracts and is torn again to a thin and long rod-like liquid drop; and in the third stage, the long rod-like droplet and the unbroken metal liquid film continue to undergo secondary breakup under the impact of the high pressure gas, which forms fine particles. Throughout the atomization process, the secondary breakup is critical for determining the final PSD of the produced powders. Therefore, considering the melt breakup mechanisms, the most extensive research related to breakup physics is the Weber criteria [19], which describe secondary atomization and are defined as follows:

$$We = \frac{\rho_g U_r^2 d_p}{\sigma} \quad (1)$$

where ρ_g is the density of gas, U_r is the relative velocity of the gas and droplet, d_p is the droplet

diameter, and σ is the surface tension of the droplet. *We* indicates the physical mechanism of secondary breakup and provides the ratio of the disrupting aerodynamic force to the restorative surface tension force, with a larger *We* indicating a higher tendency toward fragmentation.

Figure 4 presents two typical droplet breakup modes in sequence with increasing *We*. Typically, low *We* values result in the "bag break-up" process. Large droplets are blown out into the form of a hollow bag on the windward side and broken into smaller droplets at the weakest position of the bottom of the bag. With an increase in gas pressure, *We* increases. When the gas velocity substantially exceeds the critical break-up velocity, large droplets remain spherical on the windward side, but many thin sheets are stripped from the edges of the droplet surface and then broken into smaller droplets. This mechanism is known as stripping breakup.

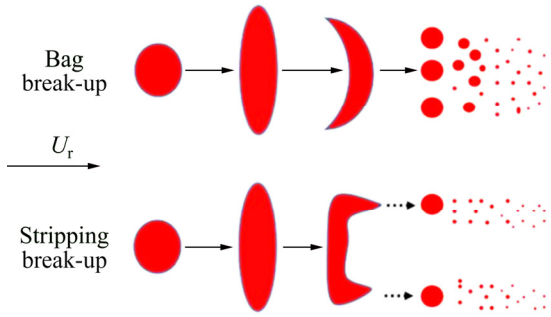

Fig. 4 Droplet breakup models

It is obvious that U_r and *We* increase with the increase of atomization pressure. A high *We* means that the secondary breakup is more sufficient and thus leads to a smaller powder size. Ti−6Al−4V powders prepared by EIGA are distributed in a wide size range from 1 to 400 μm, with an average particle size (d_{50}) of 90−145 μm. Additionally, approximately 50% of the particles are within the 50−180 μm range. Characterizations of the PSD in a batch of powder ensure that the optimum ranges of particles are used in each process. For different manufacturing processes, the optimum range of the PSD is not the same. In general, electron beam melting (EBM) uses a nominal PSD of 45−106 μm; selective laser melting (SLM) uses a finer PSD of 15−45 μm [20], while LMD uses a wide PSD range of 50−180 μm. The yields of printable powders can be expressed by the ratio of the powder with a size of 50−180 μm in relation to the total powder mass. Figure 3(b) shows the production rate of printable powder prepared at different gas pressures. With increasing gas pressure, the output of powders shows a decreasing trend after an initial increase. The highest TC4 powder yield rate of 51.6% is achieved when the gas pressure is 6.0 MPa. Thus, high pressure ensures a high yield of printable powder.

Figure 5 shows the SEM morphology of the TC4 powder prepared at different gas pressures. Although the gas pressure is different, the powders generated by the EIGA method are nominally spherical, and the proportion of irregularly shaped particles is relatively low. Some oval powders are obtained, as seen in Figs. 5(a−c); however, the number of oval powders decreases with increasing gas pressure. In the process of atomization, some broken droplets cannot solidify in time and collide with the solidified particles to form a satellite ball, as shown in Figs. 5(b, c). With increasing pressure, the content of satellite particles increases. As the pressure is up to 7.0 MPa, the pressure is so large that the powders have violent collisions with each other and form irregular particles, with some droplets even breaking into clastic particles or thin sheets by hitting the atomizing chamber wall (Fig. 5(d)).

Oval powders and satellite particles have a negative impact on the flow properties of a powder batch. The particle shape is determined by the deformation of the droplet during condensation, which is the result of competition among the external force, the surface tension and the viscous force of the droplet itself. The surface tension always tries to maintain the minimum liquid surface area, while the viscous force inhibits liquid deformation; the liquid stream will deform and break only when the external force overcomes the surface tension and the viscous force and then becomes a liquid droplet. The large droplets are unstable and will continue to deform and break under the influence of the gas flow. The spheroidization time (t_{sph}) [21] is an important factor in determining the particle shape. The shape of the powder particles depends on two factors: the contraction time of surface tension into a ball and the metal droplet solidification time (t_{sol}):

$$t_{sph} = [3\pi^2 \mu / (4V\sigma)](r_1^4 - r_2^4) \quad (2)$$

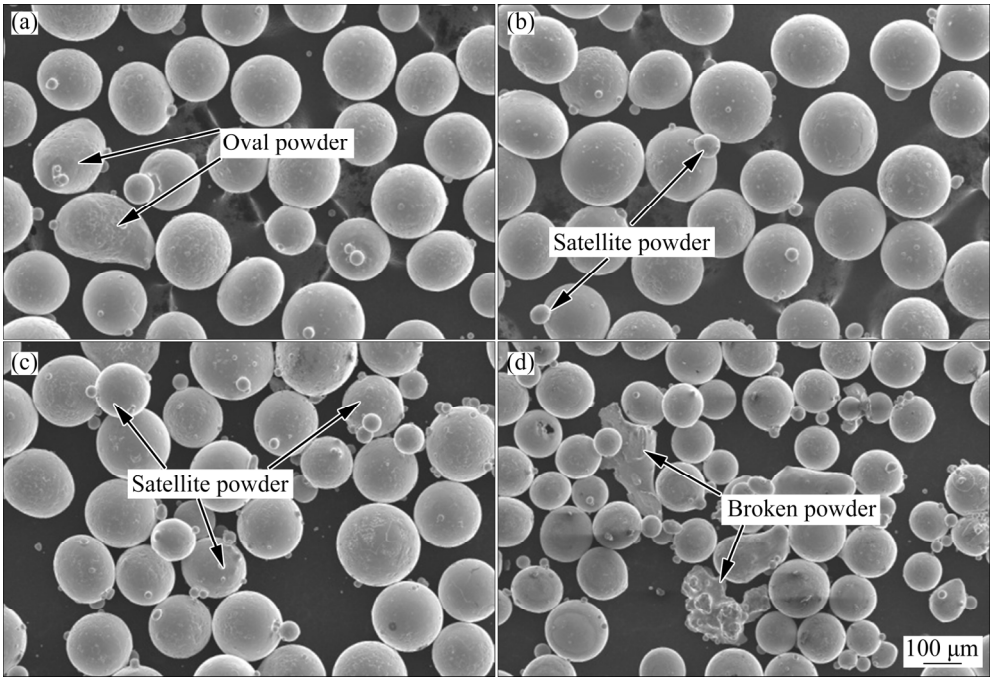

Fig. 5 SEM images of as-atomized powder prepared at different gas pressures: (a) 5.5 MPa; (b) 6.0 MPa; (c) 6.5 MPa; (d) 7.0 MPa

where μ is the viscosity, V is the volume of powder particles, σ is the surface tension of liquid metal, and r_1 and r_2 are the radii of powder particles before spheroidization and after spheroidization, respectively.

Considering that r_1 is much larger than r_2 ($r_1/r_2\approx10$) in the atomization process, the value of r_2 can be neglected, giving $V=4/3\pi r_1^3$ and simplifying Eq. (2) as follows:

$$t_{sph}=1.77(\mu/\sigma)r_1 \quad (3)$$

The cooling and solidification time of metal droplets can be expressed as [22]

$$t_{sol}=[D\rho_m/(6h)]c_p\ln[(T_m-T_o)]+H/(T_s-T_o) \quad (4)$$

where D is the droplet diameter, ρ_m is the metal solution density, h is the heat transfer coefficient, c_p is the specific heat capacity at constant pressure, T_m is the starting temperature of the metal, T_o is the atomization medium temperature, T_s is the solidification temperature, and H is the latent heat of the melting metal.

The droplet diameter (D) is inversely proportional to the gas velocity; as the pressure increases, the gas velocity increases and the droplet diameter decreases. The viscosity and surface tension of TC4 titanium alloy are 0.02 mPa·s and 1.588 N/m, respectively. When the atomization pressure is 7.0 MPa, the d_{50} of the powder is 145 μm. As seen in Eq. (3), the spheroidization time (t_{sph}) of the powder is 1.6×10^{-6} s. Relevant literature studies [23,24] show that the cooling rate of the gas atomization process is 10^2−10^6 K/s and conservatively estimates the superheat of droplets to be 500 °C. Therefore, the solidification time is not less than 10^{-5} s, which is much higher than that of the spheroidization time. Theoretically, all titanium alloy powders prepared by gas atomization should be spherical particles. However, with increasing gas pressure, the numbers of satellite particles and irregular particles increase. The main reason is that the droplets are impacted by the airstream during flight. Moreover, large particles are easily smashed in flight and collide with unsolidified droplets to form satellite balls. Thus, proper gas pressure is crucial for obtaining alloy powders with high sphericity. TC4 alloy powders (gas pressure of 6.0 MPa) are more spherical and contain fewer satellite particles.

A hollow sphere is one of the types of defects frequently found in gas atomization. Figure 6 shows images of hollow spherical powders prepared at 6.0 MPa. During the GA process, high-speed argon impacts the TC4 alloy droplet, and part of the gas flow is dispersed by the liquid alloy and bound by

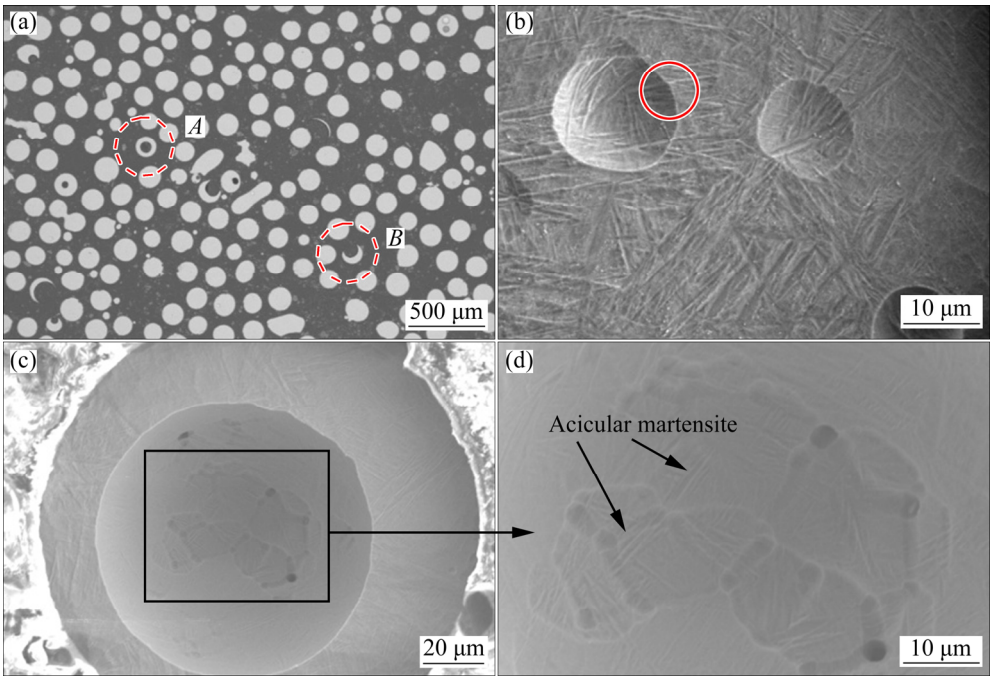

Fig. 6 SEM images of hollow powder: (a) Morphology of hollow powders by BSE; (b) Cross-section microstructure of small hole; (c) Cross-section morphology of large hole; (d) Morphology magnified from (c)

the droplet. Therefore, argon cannot escape from the droplet and form closed gas pores after solidification, as shown by *A* in Fig. 6(a). These gas pores cannot be entirely eliminated even by LMD, which is detrimental to the mechanical properties, especially fatigue properties. When the gas escapes out of the powder, the droplet cannot shrink into a solid powder and instead forms an open hollow powder, as shown by *B* in Fig. 6(a). Previous works [25,26] have also reported the occurrence of gas bubbles (a hollow powder with an inner gas) in EIGA powders. Some EIGA powder particles, especially large particles, tend to contain more gas bubbles, as shown in Fig. 6(a).

The lath martensite remains in the same direction as the martensite in the pore wall of small holes (Fig. 6(b)) because the small pore has little effect on the solidification process. The pore wall of a large hole is composed of some grains where large amounts of finer acicular martensite can be observed, and the stomatal edge appears smooth and regular, as shown in Fig. 6(c). Low-temperature gas can provide large undercooling for the pore wall, and the kinetic energy from the air bubble can provide nucleation energy and contribute to improving the nucleation rate. Therefore, the pore wall consists of many tiny grains with finer acicular martensite, as shown in Fig. 6(d). The surface relief existing in all powders results from both self-accommodation and plastic-accommodation during martensitic transformation [27].

3.2 Characteristics of TC4 powder with different particle sizes

Figure 7 shows the surface morphologies of powders prepared at 6.0 MPa. The powder surface morphology is related to the particle size. The degree of spherical shape and surface roughness for small particles are superior to those of the large particle-sized powder. The powder ranging from 150 to 180 μm has an approximately spherical morphology and a generally rough surface, with satellite particles and some irregular sphericity also visible, as shown in Fig. 7(a). The powder ranging from 1 to 50 μm exhibits a highly spherical shape and a fine surface, as shown in Fig. 7(g). In comparison with the SEM images at high magnification (Figs. 7(b, d, f, h)), some subgrains are presented in the TC4 powders, resulting in the formation of a cellular microstructure, especially in large powder particles (100−150 and 150−180 μm). This observed structure of atomized powder is the result of rapid cooling during the atomization process [3].

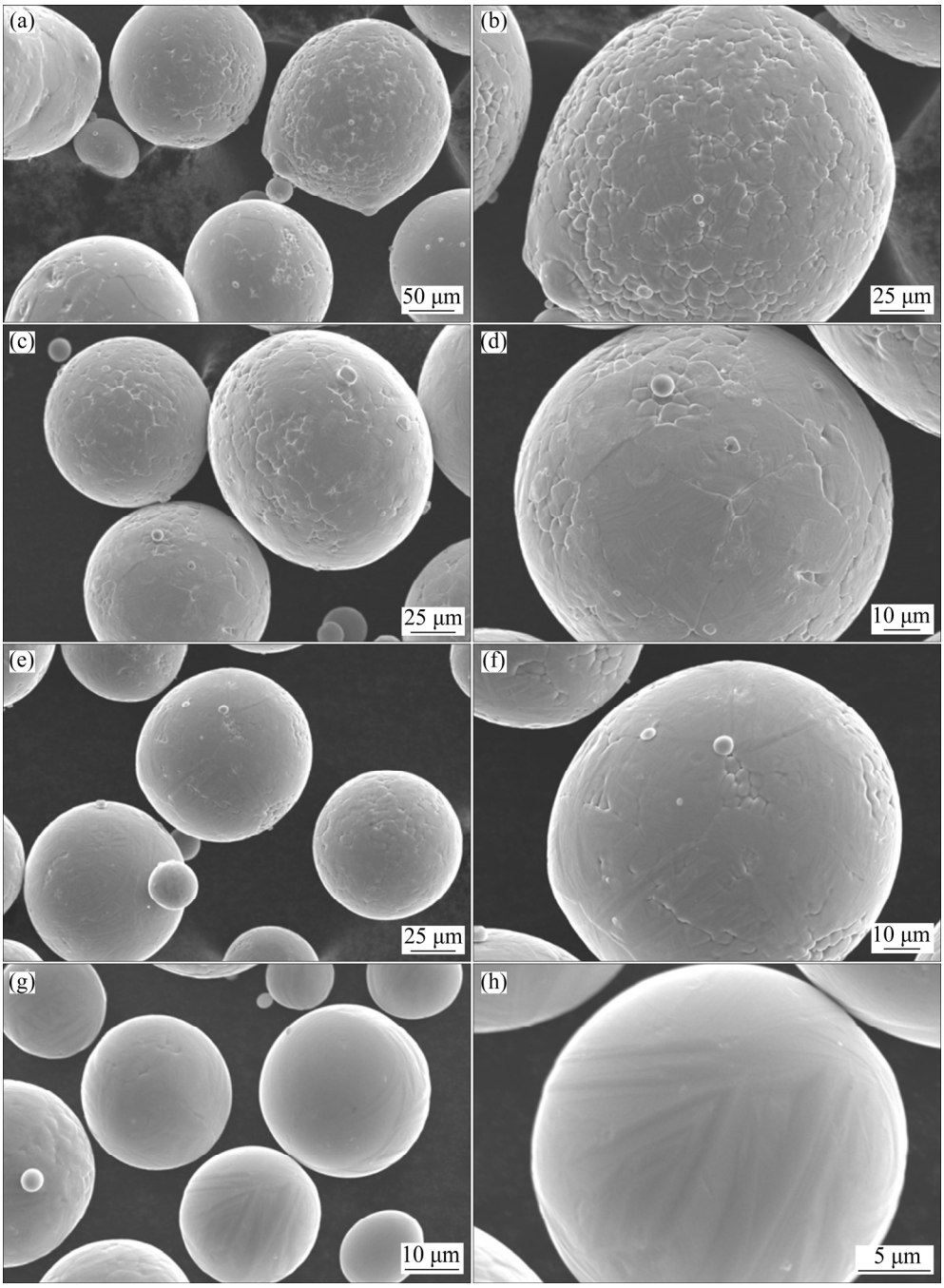

Fig. 7 SEM images of as-atomized powders with different particle sizes and representative single particle morphologies: (a, b) 150−180 μm; (c, d) 100−150 μm; (e, f) 50−100 μm; (g, h) 1−50 μm

A comparison of the surface roughness of different particle sizes at the four levels of gas pressure is presented in Fig. 8. Surface roughness tends to increase with particle size, and this increase is quicker in two powder size fractions (100−150 and 150−180 μm). With increasing pressure, a slight decrease in roughness can occur; however, when the gas pressure is 6.0 MPa, the surface roughness of the powder increases from 0.58 to 1.80 μm. The small particles show low surface roughness at all gas pressure levels.

The XRD patterns of the TC4 powder prepared at 6.0 MPa are presented in Fig. 9. The powder phase contains a close-packed hexagonal structure (α'-Ti), and the PSD seems to have no significant effect on the phase compositions. The tip of the electrode rod is heated by the induction coil and the phase of (α+β) rapidly melts into the liquid phase.

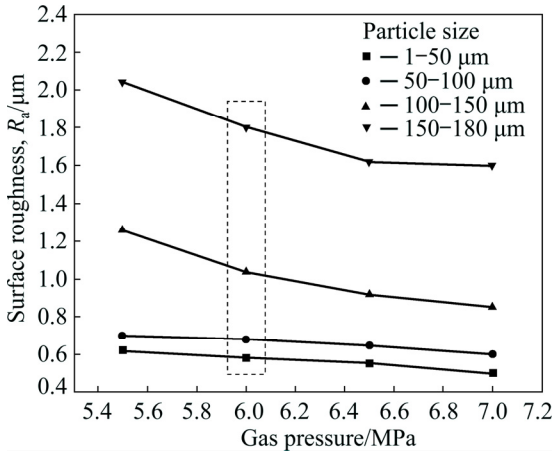

Fig. 8 Comparison of surface roughness R_a of particles with different sizes

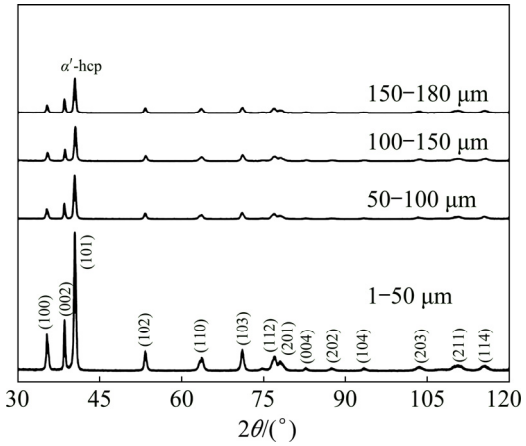

Fig. 9 X-ray diffraction patterns of atomized powders

After collisions with low-temperature argon, the liquid drop achieves a rapid solidification rate. The presence of β phase with a body center cubic (bcc) (211) crystal structure is almost diminished or absent in the LMD specimen. The low volume fraction of the β phase in the deposited region might have weak reflection. The relative concentrations of alpha (α) and beta (β) were estimated from the intensities of their reflections in the X-ray diffraction data [28]. Computational results show that the proportion of the α and β phases is 5:1. Thus, the achieved cooling rate and thermal gradient during the LMD process are attributed to the rise in the α phase and reduction in the β phase [29].

The powders with a large range in particle sizes prepared at 6.0 MPa are composed of α grains, as shown in Fig. 10, which displays cellular grains and obvious grain boundary (region A in Fig. 10(a) and region B in Fig. 10(b)). Figures 10(c) and (d) show no obvious grain boundary when the particle size decreases. The microstructures of both powders are composed of martensitic α' phases due to a rapid cooling rate (10^3−10^5 K/s). The undercooling of the small particle is higher than that of its inner surface, which leads to the droplet solidifying from its outer surface to its inner surface. Therefore, a large powder exists in many cellular grains, grain boundaries and even secondary dendrites on its surface, whereas a tiny droplet has little temperature difference between its inner surface and outer surface, which allows rapid solidification.

The apparent density and flowability of EIGA powders are summarized in Table 1. The outlet diameter of the funnel is 5.0 mm. The standard test methods for apparent density and flowability used in the experiment are ASTM B212−13 and B213−13. Except for the obvious inflation from the particle size range, the effect of the atomization pressure on the apparent density and flowability is small.

According to the standard test method, the hall flow rate (R_H) is expressed by the time required for the 50 g metal powder to flow through the standard funnel of the prescribed aperture. When the size fraction is approximately 100−150 μm and the atomized gas pressures are 6.0 and 6.5 MPa, the powders show better flowability. TC4 powder prepared at 6.5 MPa has the best flowability, and the R_H is 11.468 s. However, agglomeration is easily caused in the powder with a fine particle size (≤50 μm) because of its higher surface energy. Thus, these powders typically have poor flowability or may not flow at all [30]. This indicates that the apparent density of powder decreases with increasing particle size. However, under the effect of gas pressure, it has contrary results. Ti−6Al−4V powder with a size fraction of 1−100 μm prepared at 6.0 MPa has the highest apparent density (~2.886 g/m^3) among all the powder size fractions. The theoretical density of TC4 titanium alloy is 4.43 g/cm^3, and the ratio of apparent density is 65.1%. Therefore, the apparent density and flowability of Ti−6Al−4V powder with the size fraction (50−180 μm) prepared at 6.0 MPa are in line with the demand for LMD.

Impurity elements in titanium have a substantial influence on the comprehensive properties of titanium, especially C, N and O. Oxygen can improve the strength and hardness of

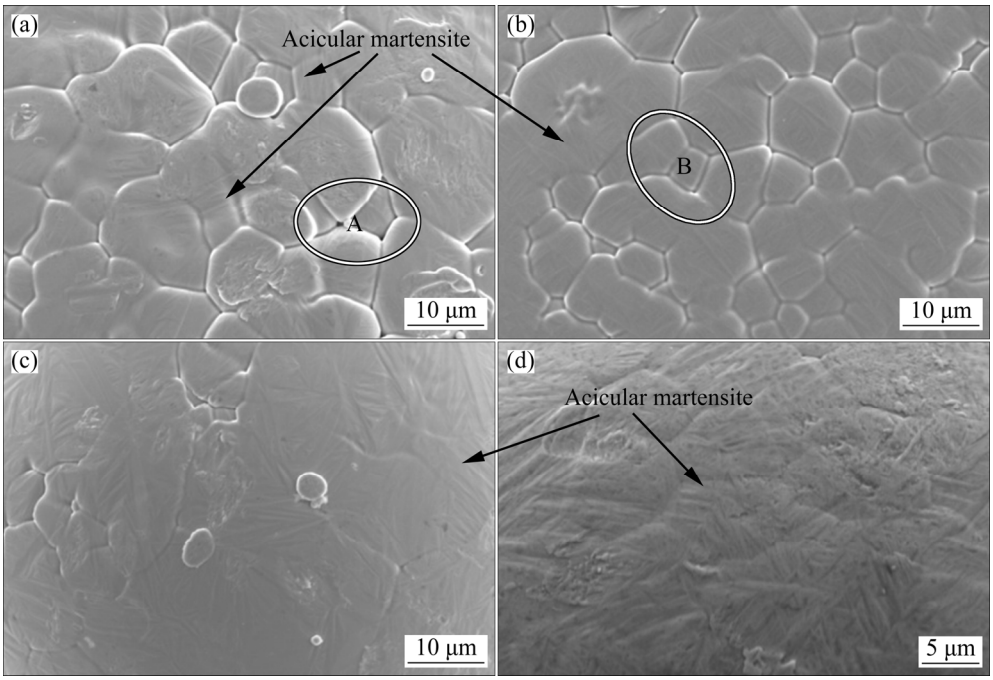

Fig. 10 Microstructures of TC4 powder with different particle sizes: (a) 150−180 μm; (b) 100−150 μm; (c) 50−100 μm; (d) 1−50 μm

Table 1 Influence of atomizing gas pressure on apparent density and flowability

Pressure/ MPa	Apparent density/(g·cm^{-3})			Flowability/s		
	1−100 μm	100−150 μm	150−180 μm	50−100 μm	100−150 μm	150−180 μm
5.5	2.778	2.772	2.669	19.455	13.477	14.925
6.0	2.886	2.785	2.651	20.661	11.655	14.620
6.5	2.865	2.791	2.639	21.459	11.468	13.966
7.0	2.813	2.809	2.631	23.041	11.990	13.441

The induction melting power is 60 kW

titanium alloy, but will seriously affect the plasticity and fracture toughness of the alloy. Although many metals are brittle at high oxygen levels, titanium is particularly sensitive to changes in trace elements. YU et al [31] found that the toughness of the Ti−0.1wt.%O sample is one-third that of the Ti−0.3wt.%O sample. Figure 11 shows the average oxygen content in powders under different pressures. With increasing gas pressure, the oxygen content in the powder increases.

Figure 12 shows the oxygen content in different particle sizes under different pressure conditions. For the powders with the same particle size, the oxygen content in the powders is consistent with the change trend of gas pressure. The oxygen content of EIGA powder (1−50 μm) prepared at 7.0 MPa is 0.168%, which is almost two

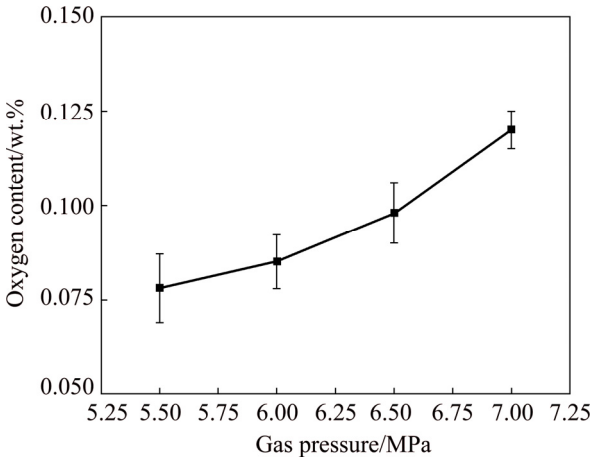

Fig. 11 Average oxygen content in powders under different pressures

times that of the particle size fractions (150−180 μm). In other words, a smaller particle size

corresponds to a higher the oxygen content because with increasing pressure, the particle size of the powder gradually decreases, which leads to a high proportion of fine powder. As a result, for a pile of powders with a fixed mass, the finer the particle size is, the higher the specific surface area, which results in an enlarged overall surface area. Therefore, the interface area between the oxygen and powder surface becomes larger, and the possibility for the combination between oxygen and titanium becomes higher. Even though the oxygen content in the powder increases, the increase is not substantial. The oxygen content still remains in the low range of 0.06%−0.20%. The reason for this may be that the atomization medium used in the experiment is high-purity argon, which avoids the increase in oxygen in the atomization process. In addition, the vacuum system uses a three-stage pumping system including a mechanical pump, root pump and diffusion pump. The use of the diffusion pump greatly improves the vacuum degree of the atomizing chamber, and the vacuum limit can reach 3×10^{-3} Pa. Therefore, using both devices greatly reduces the oxygen enrichment phenomenon in the atomization process and ensures that the oxygen content of the Ti−6Al−4V alloy powder remains in a reasonable range.

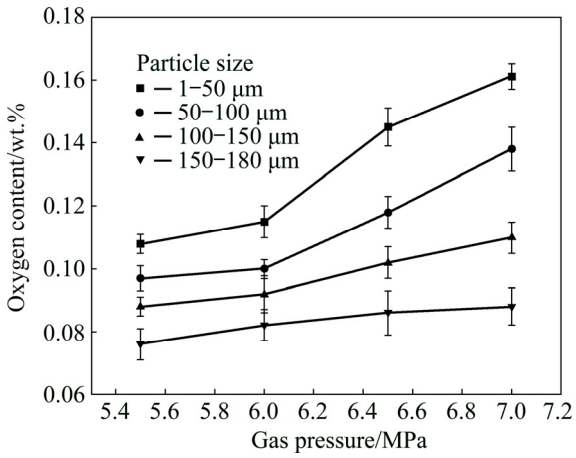

Fig. 12 Oxygen content in different particle sizes under different pressure conditions

3.3 Microstructure and properties of LMD specimens

The apparent density and flowability of the powders are important technological parameters, which directly affect the LMD process [32,33]. The particle size fraction (50−180 μm) was screened to evaluate the 3D printing capability of EIGA powders. Laser diffraction and Holzer flow meter analysis of the powder samples reveal that the powder prepared at higher pressures has a larger mean particle diameter, but for flowability, the opposite trend is observed (Table 2).

Table 2 Properties of EIGA powders with particle sizes of 50−180 μm

Pressure/MPa	Mean particle diameter/μm	Powder size, d_{90}/μm	Flowability/s
5.5	90	161	15.178
6.0	82	152	16.720
6.5	75	146	18.015
7.0	68	143	19.342

The microstructure of the deposited sample is shown in Fig. 13(a), wherein the long prior β grains are observed in the laying direction. The phase of Ti−6Al−4V is mainly composed of α+β grains with a fine lamellar Widmanstatten structure. Furthermore, most of grains exist in the β transformation phase (α+β plates), as shown in Fig. 13(b). These results indicate that the cooling rate of the part during laser deposition is above the β transus temperature, and it is not sufficiently fast to allow the formation of martensite, which is consistent with the microstructures previously reported in the as-fabricated AM parts [34].

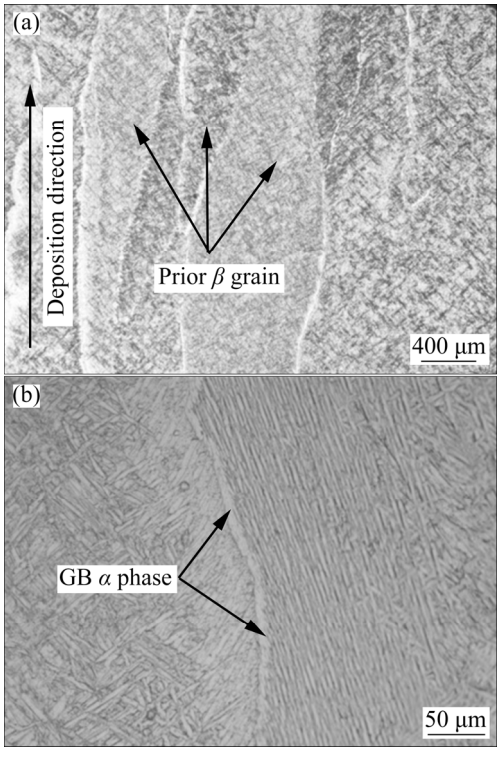

Fig. 13 Microstructures of TC4 alloy fabricated by LMD

The tensile properties of the TC4 alloy specimens are shown in Fig. 14. It is found that both ultimate tensile strength and yield strength for all four types of specimens are around at the same level, which are approximately 1100 and 1000 MPa, respectively. However, the ductility shows an obvious increase with gas pressure. Generally, the parts manufactured using powders prepared at 7.0 MPa have good strength and ductility. The results suggest that the variation in powder type does not significantly influence the tensile strength of the as-prepared part.

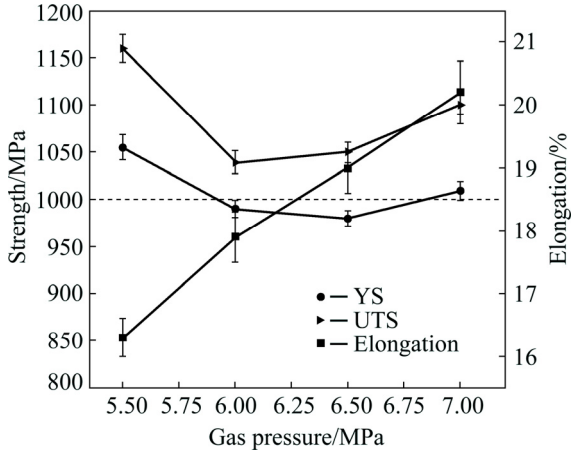

Fig. 14 Mechanical properties of TC4 alloy under different gas pressures

A summary of relevant mechanical properties of Ti−6Al−4V alloys reported in the literature is listed in Table 3. It is noted that LMD-processed Ti−6Al−4V shows increased tensile strength compared to that of the cast or wrought material. Compared with the sample deposited in the same manufacturing process [34], the strength values are proportional to those of the LMD specimens. Additionally, the ductility of the specimens (6.5 and 7.0 MPa) measured in the present study are even slightly higher than those found in previous studies on the as-produced Ti−6Al−4V fabricated through LMD (7.0 MPa), and the elongation reaches 20.2%. In conclusion, the samples fabricated by LMD using EIGA powders have good comprehensive mechanical properties. Powders prepared with proprietary equipment (EIGA) have a favorable 3D printing capability.

Table 3 Contrast of mechanical properties of TC4 alloy with different manufacturing processes

Process	Source	Condition	YS/ MPa	UTS/ MPa	Elongation/ %
Cast	ASTM F1108 [35]	–	758	860	>8
	DONACHIE [36]	As-fabricated	896	1000	8
Wrought	ASTM F1472 [37]	–	860	930	>10
	DONACHIE [36]	β-solution treated	931	1055	9
LMD (AM)	CARROLL et al [34]	As-fabricated	945± 13	1041± 12	18.7± 1.7

4 Conclusions

(1) Ti−6Al−4V alloy powder was achieved using a self-developed EIGA system. All the prepared Ti−6Al−4V alloy powders under four atomization gas pressures are nominally spherical, and the proportion of irregularly shaped particles is relatively low.

(2) The powders prepared at gas pressures of 6.0 and 6.5 MPa, with a size fraction of 100−150 μm, have better flowability. The oxygen content is consistent with the change trend of gas pressure and remains within a low range of 0.06%−0.20%.

(3) TC4 specimens fabricated by LMD are mainly composed of α+β grains with a fine lamellar Widmanstatten structures and have the same UTS and yield strength of approximately 1100 and 1000 MPa, respectively. Elongation of the samples can reach 20.2% at a gas pressure of 7.0 MPa.

(4) The processed powders have a favorable 3D printing capability, and the properties of Ti−6Al−4V alloys manufactured by LMD using EIGA powders typically exceed those of their cast or wrought counterparts.

References

[1] HERZOG D, SEYDA V, WYCISK E, EMMELMANN C. Additive manufacturing of metals [J]. Acta Materialia, 2016, 117: 371−392.

[2] DUTTA B, (SAM) FROES F H. The additive manufacturing (AM) of titanium alloys [J]. Metal Powder Report, 2017, 72: 96−106.

[3] YANG D Y, GUO S, PENG H X, CAO F Y, LIU N, SUN J F. Size dependent phase transformation in atomized TiAl powders [J]. Intermetallics, 2015, 61: 72−79.

[4] HEIDLOFF A J, RIEKEN J R, ANDERSON I E, BYRD D, SERAS J, GLYNN M, WARD R M. Advanced gas atomization processing fot Ti and Ti alloy powder

manufacturing [J]. JOM, 2010, 62: 35−41.

[5] ANTONY L V M, REDDY R G. Processes for production of high-purity metal powders [J]. JOM, 2003, 55: 14−18.

[6] LIU Z Q, HUANG C S, GAO C F, LIU R P, CHEN J, XIAO Z Y. Characterization of Ti6Al4V powders produced by different methods for selective electron beam melting [J]. Journal of Mining and Metallurgy, Section B: Metallurgy, 2019, 55(1): 121−128.

[7] CHEN Wen-mi, WAN Xin-hua. Effect of structure of nozzle and processing parameters on particle size of zinc powders in gas atomization [J]. The Chinese Journal of Nonferrous Metals, 2001, 11(5): 852−857. (in Chinese)

[8] AKSOY A , UNAL R. Effects of gas pressure and protrusion length of melt delivery tube on powder size and powder morphology of nitrogen gas atomised tin powders [J]. Powder Metallurgy, 2006, 49(4): 349−354.

[9] ZHAO X M, XU J, ZHU X X, ZHAO S M. Effect of closed-couple gas atomization pressure on the performances of Al−20Sn−1Cu powders [J]. Rare Metals, 2008, 27(4): 439−443.

[10] RAJU R, DURAISELVAM M, PETLEY V, VERMA S, RAJENDRAN R. Microstructural and mechanical characterization of Ti6Al4V refurbished parts obtained by laser metal deposition [J]. Materials Science and Engineering A, 2015, 643: 64−71.

[11] MAHAMOOD R M, AKINLABI E T. Effect of laser power and powder flow rate on the wear resistance behaviour of laser metal deposited TiC/Ti6Al4V composites [J]. Materials Today Proceeding, 2015, 2: 2679−2686.

[12] SPIERINGS A B, VOEGTLIN M, BAUER T, WEGENER K. Powder flowability characterisation methodology for powder-bed- based metal additive manufacturing [J]. Progress in Additive Manufacturing, 2016, 1(1−2): 9−20.

[13] FROES F H. Titanium powder metallurgy: A review – Part 1 [J]. Advanced Materials & Processes, 2012, 170(9): 16−22.

[14] AHSAN M N, PINKERTON A J, MOAT R J, SHACKLETON J. A comparative study of laser direct metal deposition characteristics using gas and plasma-atomized Ti−6Al−4V powders [J]. Materials Science and Engineering A, 2011, 528: 7648−7657.

[15] GUO R P, XU L, ZONG Y P, YANG R. Characterization of prealloyed Ti−6Al−4V powders from EIGA and PREP process and mechanical properties of HIPed powder compacts [J]. Acta Metallurgica Sinica (English Letters), 2017, 30(8): 1−10.

[16] MI J, FIGLIOLA R S, ANDERSON I E. A numerical simulation of gas flow field effects on high pressure gas atomization due to operating pressure variation [J]. Materials Science and Engineering A, 1996, 208: 20−29.

[17] GAO C F, XIAO Z Y, ZOU H P, LIU Z Q, CHEN J, LI S K, ZHANG D T. Characterization of spherical AlSi10Mg powder produced by double-nozzle gas atomization using different parameters [J]. Transactions of Nonferrous Metals Society of China, 2019, 29: 374−384.

[18] UNAL A. Liquid break-up in gas atomization of fine aluminum powders [J]. Metallurgical Transactions B (Process Metallurgy), 1989, 20(1): 61−69.

[19] ASHGRIZ N, YARIN A L. Capillary instability of free liquid jets [M]//Handbook of Atomization and Sprays. Springer US, 2011.

[20] DAWES J, BOWERMAN R, TREPLETON R. Introduction to the additive manufacturing powder metallurgy supply chain [J]. Johnson Matthey Technol Rev, 2015, 59(3): 243−256.

[21] LAVERNIA E J, AYERS J D, SRIVATSAN T S. Rapid solidification processing with specific application to aluminium alloys [J]. Metallurgical Reviews, 1992, 37(1): 1−44.

[22] SEE J B, JOHNSTON G H. Interactions between nitrogen jets and liquid lead and tin streams [J]. Powder Technology, 1978, 21(1): 119−133.

[23] ZHENG B, LIN Y, ZHOU Y, LAVERNIA E J. Gas atomization of amorphous aluminum: Part I. Thermal behavior calculations [J]. Metallurgical and Materials Transactions B, 2009, 40: 768−778.

[24] CIFTCI N, ELLENDT N, COULTHARD G, SOARES BARRETO E, MADLER L, UHLENWINKEL V. Novel cooling rate correlations in molten metal gas atomization [J]. Metallurgical and Materials Transactions B, 2019, 55: 666−677.

[25] GUO R P, XU L, WU J, YANG R, ZONG Y P. Microstructural evolution and mechanical properties of powder metallurgy Ti−6Al−4V alloy based on heat response [J]. Materials Science and Engineering A, 2015, 639: 327−334.

[26] WEGMANN G, GERLING R, SCHIMANSKY F P. Temperature induced porosity in hot isostatically pressed gamma titanium aluminide alloy powders [J]. Acta Materialia, 2003, 51: 741−752.

[27] ZHAO Shao-yang, CHEN Gang, TAN Ping, WANG Jian, LIU Xiao-qing. Characterization of spherical TC4 powders by gas atomization and its interstitial elemental control [J]. The Chinese Journal of Nonferrous Metals, 2016, 26(5): 980−987. (in Chinese)

[28] BALLA V K, SODERLIND J, BOSE S, BANDYOPADHYAY A. Microstructure, mechanical and wear properties of laser surface melted Ti6Al4V alloy [J]. Journal of the Mechanical Behavior of Biomedical Materials, 2014, 32(4): 335−344.

[29] AL-BERMANI S S, BLACKMORE M L, ZHANG W, TODD I. The origin of microstructural diversity, texture, and mechanical properties in electron beam melted Ti−6Al−4V [J]. Metallurgical and Materials Transactions A (Physical Metallurgy and Materials Science), 2010, 41: 3422−3434.

[30] GAMBLE J F, CHIU W S, TOBYN M. Investigation into the impact of sub-populations of agglomerates on the particle size distribution and flow properties of conventional microcrystalline cellulose grades [J]. Pharmaceutical Development and Technology, 2011, 16(5): 542−548.

[31] YU Q, QI L, TSURU T, TRAYLOR R, RUGG D, MORRIS J W, ASTA M, CHRZAN D C, MINOR A M. Origin of dramatic oxygen solute strengthening effect in titanium [J]. Science, 2015, 347: 635−639.

[32] WEI W H, WANG L Z, CHEN T, DUAN X M, LI W. Study on the flow properties of Ti−6Al−4V powders prepared by radio-frequency plasma spheroidization [J]. Advanced Powder Technology, 2017, 28(9): 2431−2437.

[33] ZHU H H, FUH J Y H, LU L. The influence of powder apparent density on the density in direct laser-sintered metallic parts [J]. International Journal of Machine Tools and Manufacture, 2007, 47(2): 294−298.
[34] CARROLL B E, PALMER T A, BEESE A M. Anisotropic tensile behavior of Ti−6Al−4V components fabricated with directed energy deposition additive manufacturing [J]. Acta Materialia, 2015, 87: 309−320.
[35] ASTM F1108-14. Standard specification for titanium−6aluminum−4vanadium alloy castings for surgical implants (UNS R56406) [S]. 2014.
[36] DONACHIE M J. Titanium: A technical guide [M]. 2nd Edition. Materials Park: ASM International, 2000.
[37] ASTM F1472-14. Standard specification for wrought titanium−6aluminum−4vanadium alloy for surgical implant applications (UNS R56400) [S]. 2014.

高压 EIGA 法制备 Ti−6Al−4V 合金粉末及其 3D 可打印性

郭快快[1,2]，刘常升[1,2]，陈岁元[1,2]，董欢欢[1,2]，王思宇[1,2]

1. 东北大学 材料科学与工程学院，沈阳 110819；
2. 东北大学 激光应用技术与装备辽宁省重点实验室，沈阳 110819

摘　要：采用电极感应熔炼气雾化(EIGA)设备制备 Ti−6Al−4V 合金粉末，研究高压(5.5~7.0 MPa)雾化压力对粉末特性和显微结构的影响，并分析激光打印(LMD)件的力学性能。结果表明：所制备的粉末粒径分布在 1～400 μm，随着雾化压力的增加，粉末的平均粒径逐渐减小。在气压 6.0 和 6.5 MPa 下制备的粒径分布在 100~150 μm 范围内的粉末具有较好的流动性。粉末的氧含量随着压力的升高而增加，但均在 0.06%~0.20%较低范围内。LMD 制备的 TC4 试样主要由具有魏氏结构的 α 和 β 两相组成，其极限抗拉强度和屈服强度分别约为 1100 MPa 和 1000 MPa。EIGA 法制备的钛合金粉末具有良好的 3D 可打印性，LMD 制备的 TC4 合金的力学性能超过铸造或锻造件的。

关键词：Ti−6Al−4V 粉末；高压气雾化；粒径；流动性；3D 可打印性

(Edited by Bing YANG)